An Amplitude Modulation Detector for Fault Diagnosis in Rolling Element Bearings

Jason R. Stack, *Member, IEEE*, Ronald G. Harley, *Fellow, IEEE*, and Thomas G. Habetler, *Fellow, IEEE*

***Abstract*—The purpose of this research is to identify single-point defects in rolling element bearings. These defects produce characteristic fault frequencies that appear in the machine vibration and tend to modulate the machine's frequencies of mechanical resonance. An amplitude modulation (AM) detector is developed to identify these interactions and detect the bearing fault while it is still in an incipient stage of development (*i.e.*, to detect the instances of AM when the magnitude of the characteristic fault frequency itself is not significant). Use of this detector only requires machine vibration from one sensor and knowledge of the bearing characteristic fault frequencies. Computer simulations as well as machine vibration data from bearings containing outer race faults are used to confirm the proficiency of this proposed technique.**

***Index Terms*—Amplitude modulation (AM), bearings (mechanical), bispectrum, condition monitoring, fault diagnosis, vibration.**

I. Introduction

ELECTRIC machine failures are divided into stator, rotor, and bearing faults. Approximately half of all electric machine failures are due to bearing faults [1]–[4]; therefore, the ability to predict the onset of a bearing failure is of great practical importance. The methods of bearing condition monitoring are diverse but can be categorized by the type of measurement that is performed. Examples of measured parameters include current, vibration, temperature, and displacement. The objective of this research is to identify bearing faults via machine vibration while the fault is still in an incipient stage.

II. Bearing Fault Signatures

Single-point defects commonly occur as pits or spalls on a bearing surface. This type of defect will produce one of the four characteristic fault frequencies in the machine vibration depending on which bearing surface contains the fault. These frequencies are illustrated in Fig. 1, where

F_R rotor (shaft) frequency;
F_{CF} cage fault frequency;
F_{IRF} inner raceway fault frequency;
F_{ORF} outer raceway fault frequency;
F_{BF} ball fault frequency;
D_B ball diameter;

Manuscript received December 12, 2002; revised June 22, 2004. Abstract published on the Internet July 15, 2004. This paper was presented at the 28th Annual Conference of the IEEE Industrial Electronics Society, Seville, Spain, November 5–8, 2002.

J. R. Stack is with Signal and Image Processing, Naval Surface Warfare Center, Panama City FL 32407 USA (e-mail: jason.stack@navy.mil).

R. G. Harley and T. G. Habetler are with the Electrical and Computer Engineering Department, Georgia Institute of Technology, Atlanta, GA 30332 USA (e-mail: ron.harley@ece.gatech.edu; thabetler@ee.gatech.edu).

Digital Object Identifier 10.1109/TIE.2004.834971

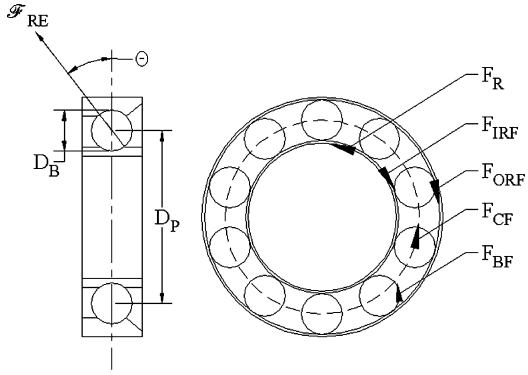

Fig. 1. Dimensions and frequencies related to bearing faults signatures.

D_P pitch diameter;
N_B number of rolling elements;
$\mathcal{F}_{\mathrm{RE}}$ direction of force exerted by the rolling element on the outer raceway;
θ ball contact angle.

The characteristic fault frequencies can be calculated using (1)–(4) [5], and a derivation of these equations is presented in [6]

$$F_{\mathrm{CF}} = \frac{1}{2} F_R \left(1 - \frac{D_B \cos(\theta)}{D_P}\right) \tag{1}$$

$$F_{\mathrm{ORF}} = \frac{N_B}{2} F_R \left(1 - \frac{D_B \cos(\theta)}{D_P}\right) \tag{2}$$

$$F_{\mathrm{IRF}} = \frac{N_B}{2} F_R \left(1 + \frac{D_B \cos(\theta)}{D_P}\right) \tag{3}$$

$$F_{\mathrm{BF}} = \frac{D_P}{2D_B} F_R \left(1 - \frac{D_B^2 \cos^2(\theta)}{D_P^2}\right). \tag{4}$$

These equations require detailed knowledge of the bearing geometry; therefore, some researchers [7] have proposed approximations (5) and (6). However, (5) and (6) approximate the ratio D_B/D_P and only give accurate characteristic fault frequency predictions for some bearing types (*e.g.*, they are valid for 6200-series bearings but not for 6300-series bearings).

$$F_{\mathrm{ORF}} = 0.4 * N_B * F_R \tag{5}$$

$$F_{\mathrm{IRF}} = 0.6 * N_B * F_R. \tag{6}$$

Single-point defects begin as localized defects on the raceways (or rolling elements), and, as the rolling elements pass over these defect areas, small collisions occur producing mechanical shockwaves. These shockwaves then excite the frequencies of natural mechanical resonance in the machine. This process occurs every time a defect collides with another part of the bearing, and its rate of occurrence is equal to one of the previously defined characteristic fault frequencies. Re-

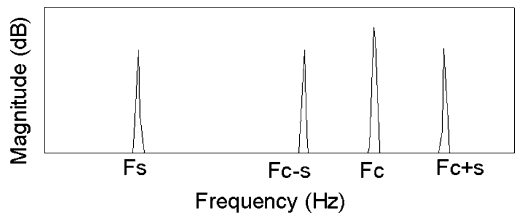

Fig. 2. Basic amplitude modulation in the frequency domain where F_S and F_C interact to generate sum and difference components.

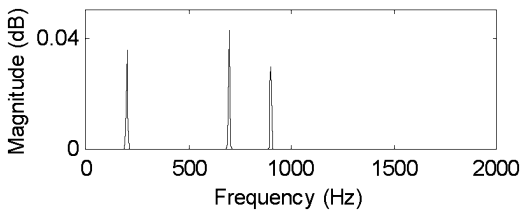

Fig. 3. The power spectrum estimate indicates the presence of a sum frequency at 900 Hz, but the origin of this component cannot be determined from this figure.

stated, inserting familiar terminology, the mechanical resonant frequencies (carriers) are modulated by the characteristic fault frequency (baseband signal). A frequency-domain representation of amplitude modulation (AM) is depicted in Fig. 2 where F_S is the baseband signal component and F_C is the carrier frequency. In this illustration, a component with frequency F_S and phase ϕ_S interacts with another component at F_C, ϕ_C to produce two new sideband components at F_{C+S}, ϕ_{C+S} and F_{C-S}, ϕ_{C-S}. Because the phases of the two sideband components are related to the phases of F_C and F_S (i.e., they are sum phases and difference phases), this type of interaction is generally referred to as quadratic phase coupling (QPC).

III. Detection of AM and QPC

Standard tools for the detection of QPC are the bispectrum and its normalized form, the squared bicoherence [8]. These estimates are defined in (7) and (8), respectively, where $X(\cdot)$ is the Fourier transform. $E\{\cdot\}$ is the statistical expectation operator, and $*$ denotes complex conjugation. While the definition of the bispectrum in (7) is standard, the names and definitions of bicoherence vary among the literature. A summary of the various bicoherence estimators can be found in [9]. The definition of squared bicoherence used in (8) is chosen because it is bounded between 0–1

$$B(f_1, f_2) = E\left\{X(f_1)X(f_2)X^*(f_1+f_2)\right\} \tag{7}$$

$$b^2(f_1, f_2) = \frac{|B(f_1, f_2)|^2}{E\left\{|X(f_1)X(f_2)|^2\right\} E\left\{|X(f_1+f_2)|^2\right\}}. \tag{8}$$

The bispectrum and bicoherence have been employed in detecting QPC in a wide variety of applications including plasma, ocean noise, and bearing faults [10]–[15]. Consider the following example of QPC detection where only a sum frequency is present:

$$x(n) = 0.8\sin(2\pi 200n + \phi_1) + \sin(2\pi 700n + \phi_2) + 0.8\sin(2\pi 900n + \phi_3) + w(n). \tag{9}$$

In this expression, $w(n)$ is -40 dB white Gaussian noise and $\phi_3 = \phi_1 + \phi_2$. It is desired to determine if the 900-Hz component is generated by an interaction between the 200- and 700-Hz components or if it is a result of some unrelated, independent source. By inspecting the power spectrum estimate in Fig. 3 (computed via Welch's method) the origin of the 900-Hz component cannot be determined. In an effort to understand the origin of the 900-Hz component, the bispectrum is calculated and shown in Fig. 4(a).

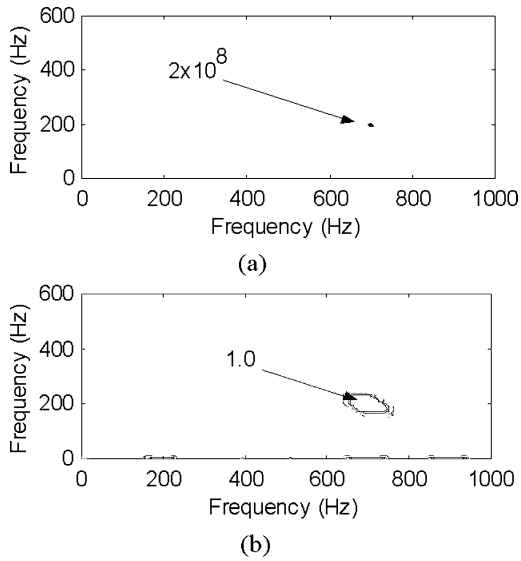

Fig. 4. Detection of QPC. (a) Contour plot of the bispectrum demonstrates a peak at (200 Hz, 700 Hz). This indicates the sum frequency component is generated by QPC. Only significant peaks are shown for clarity. (b) Contour plot of the squared bicoherence. Since the magnitude of this peak is 1.0, all of the energy at the sum frequency is due to QPC.

The bispectrum is typically displayed as a three-dimensional plot with frequency on the x and y axes and magnitude on the z axis. For simplicity and clarity, this paper uses two-dimensional contour plots to show frequency on the horizontal and vertical axes with magnitude coming out of the page. In Fig. 4(a), the presence of the peak at frequency pair (200 Hz, 700 Hz) indicates that these two components are indeed interacting to generate the 900-Hz component. However, the magnitude of this peak (2×10^8) does not reveal how much of the energy at 900 Hz is due to the interaction of the components at 200 and 700 Hz versus how much could be due to some additional independent 900-Hz source. Thus, the squared bicoherence is computed in Fig. 4(b), and, since the magnitude of its peak is equal to 1.0, it is concluded that all of the energy in the 900 Hz component is due to the interaction of the 200- and 700-Hz components.

Two details about these plots should be noted. First, the bispectrum exhibits many symmetries including $B(f_1, f_2) = B(f_2, f_1)$; therefore, it is not necessary to compute every frequency pair. A good discussion of bispectrum symmetries and its region of computation is provided in [8], [10], and [12]. Second, the resolution of the squared bicoherence in Fig. 4(b) may not be sufficient to resolve frequency components in certain applications. Therefore, many techniques are available

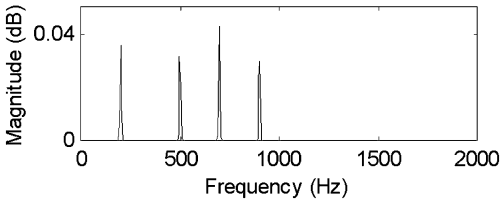

Fig. 5. Power spectrum estimate indicating the presence of a sum frequency (900 Hz) and a difference frequency (500 Hz). Again, the origin of these components cannot be determined from the power spectrum.

to improve the resolution of the estimators in (7) and (8), and these methods are discussed in [8], [9], and [16].

This example could be continued by considering the case where ϕ_3 is uncorrelated with $\phi_1 + \phi_2$. This would represent a situation where it is only coincidental that the 900-Hz component occurs at the sum frequency of the other two components. The power spectrum for this situation would be identical to Fig. 3. However, the peak in the bispectrum of Fig. 4(a) would be significantly reduced, and there would be no peak in the squared bicoherence of Fig. 4(b).

The bispectrum can also be applied to the detection of AM; however, incorrect and misleading results are often produced as the following example illustrates. Fig. 5 shows the power spectrum estimate for the signal

$$\begin{aligned} x(n) = {} & 0.8\sin(2\pi 200n + \phi_1) + \sin(2\pi 700n + \phi_2) \\ & + 0.8\sin(2\pi 900n + \phi_2 + \phi_1) \\ & + 0.8\sin(2\pi 500n + \phi_2 - \phi_1) + w(n). \end{aligned} \tag{10}$$

This signal represents a typical example of AM where two frequencies (200 and 700 Hz) interact to produce a sum-frequency component (900 Hz) and difference-frequency component (500 Hz). From the expression for the bispectrum in (7), it is observed that this estimator searches only for the presence of a sum frequency. Consequently, it not only correctly recognizes that the 900-Hz component is produced by the 200- and 700-Hz components, but it also incorrectly suggests that the 200-Hz component and the 500-Hz component are interacting to generate the 700-Hz component (i.e., $700\,\text{Hz} = 200\,\text{Hz} + 500\,\text{Hz}$) in Fig. 6. This makes the interpretation of the bispectrum difficult and confusing when used in the presence of AM. While the authors in [17] have proposed modifying the bispectrum to detect instances of AM, their modifications do not solve the problem of multiple peaks per instance of AM illustrated in this example.

While this example illustrates one disadvantage of using the bispectrum in the presence of AM, this research considers yet another disadvantage, which is specific to bearing fault diagnosis. In AM due to bearing faults, the carrier frequency and its sideband components occur in regions of natural mechanical resonance; therefore, these frequency components are salient in machine vibration. However, the characteristic fault frequencies are determined by bearing geometry, and they typically occur at low frequencies where significant mechanical damping may be present. Therefore, by the time the energy at these characteristic fault frequencies propagates from the bearing to the vibration sensor, they can be significantly attenuated. This phenomenon is especially noticeable in incipient bearing faults where the energy at the characteristic fault frequencies is low. This produces

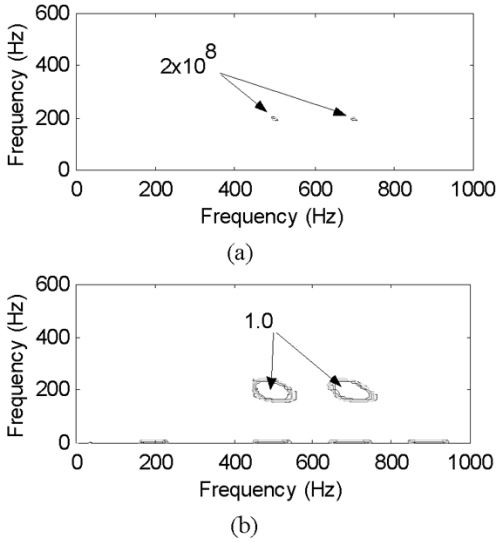

Fig. 6. Incorrect detection of AM. (a) The bispectrum shows one correct peak at (200 Hz, 700 Hz) and an additional incorrect peak at (200 Hz, 500 Hz). (b) The squared bicoherence shows the same incorrect peaks.

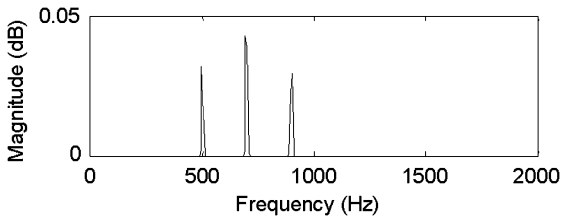

Fig. 7. Power spectrum estimate of AM generated by a bearing fault where the characteristic fault frequency (200 Hz) is significantly attenuated.

the type of AM depicted in Fig. 7 where the carrier (700 Hz) and its sidebands are significant but the magnitude of the characteristic fault frequency (200 Hz) is severely attenuated.

The damping of the characteristic fault frequency illustrated in Fig. 7 combined with the bispectrum's tendency to produce false peaks depicted in Fig. 6 suggest the need for a new AM detector. An AM detector that accounts for both of these limitations is proposed in (11) and its normalized form is defined in (12)

$$\begin{aligned} & D(f_1, f_2) \\ & \quad = E\left\{X(f_2 + f_1)X(f_2 - f_1)X^*(f_2)X^*(f_2)\right\} \end{aligned} \tag{11}$$

$$\begin{aligned} & d(f_1, f_2) \\ & \quad = \frac{|D(f_1, f_2)|^2}{E\left\{\left|X(f_2)X(f_2)\right|^2\right\} E\left\{\left|X(f_2 + f_1)X(f_2 - f_1)\right|^2\right\}}. \end{aligned} \tag{12}$$

From (11), it is seen that this AM detector searches for the carrier, sum, and difference frequencies, but does not require the presence of the baseband signal (characteristic fault frequency). To illustrate the operation of this detector the right-hand side of (11) can be expanded as follows:

$$\begin{aligned} E\Big\{ & |X(f_2 + f_1)|e^{j\angle X(f_2+f_1)}|X(f_2 - f_1)|e^{j\angle X(f_2-f_1)} \\ & \cdot|X(f_2)|e^{-j\angle X(f_2)}|X(f_2)|e^{-j\angle X(f_2)}\Big\}. \end{aligned} \tag{13}$$

Collecting like terms yields

$$E\{|X(f_2+f_1)||X(f_2-f_1)||X(f_2)||X(f_2)| \cdot e^{j[\angle X(f_2+f_1)+\angle X(f_2-f_1)-\angle X(f_2)-\angle X(f_2)]}\}. \quad (14)$$

If there is phase coupling between the sideband components f_1 and f_2, then

$$\angle X(f_2+f_1) = \angle X(f_2) + \angle X(f_1) \quad (15a)$$
$$\angle X(f_2-f_1) = \angle X(f_2) - \angle X(f_1). \quad (15b)$$

By substituting (15a) and (15b) into (14), it can be seen that the phase of (14) will equal zero, and (14) will equal the expected value of the product of the magnitudes. Therefore, if significant frequency components exist at f_{2-1}, f_{2+1}, and f_2, the detector will exhibit a peak at $D(f_1, f_2)$ indicating that frequencies f_1 and f_2 are interacting to produce sideband components.

On the other hand, if there is no phase coupling between any of the components, (15) is not valid, and the phase of (14) will vary randomly from sample to sample. The expectation operator will then cause the value of $D(f_1, f_2)$ to approach zero after a sufficient number of samples are averaged together. Therefore, the AM detector will not exhibit a peak at $D(f_1, f_2)$ if no phase coupling is present.

This estimator will also correctly produce only one peak per occurrence of AM. The normalized version of the detector in (12) is bounded between 0–1, which can be shown by application of Cauchy's inequality.

To illustrate the effectiveness of the proposed AM detector on a simple signal consider the following:

$$x(n) = 0.01\sin(2\pi 200n + \phi_1) + \sin(2\pi 700n + \phi_2) + 0.8\sin(2\pi 900n + \phi_2 + \phi_1) + 0.8\sin(2\pi 500n + \phi_2 - \phi_1) + w(n). \quad (16)$$

This example is indicative of AM in faulty bearing vibration data where the characteristic fault frequency (200 Hz) is severely attenuated (e.g., an incipient bearing fault) and the additive white Gaussian noise $w(n)$ is approximately equal in magnitude to the other components. The power spectrum estimate for this signal is illustrated in Fig. 7. If the squared bicoherence were applied to this signal, it would not exhibit any peaks, thereby failing to identify the presence of any QPC or AM. The AM detector correctly identifies the frequency pair at (200 Hz, 700 Hz) as generating the AM in Fig. 8(a). The normalized AM detector of Fig. 8(b) confirms all of the energy at the sidebands is due to the interaction of the 200- and 700-Hz components.

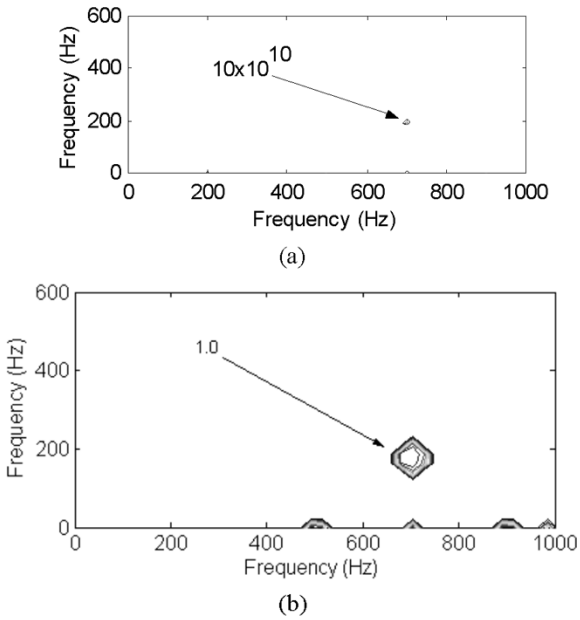

Fig. 8. Successful detection of AM. (a) The proposed AM detector correctly identifies the source components at (200 Hz, 700 Hz) despite the characteristic fault frequency being significantly attenuated. (b) The normalized form of the proposed AM detector correctly suggests all energy at the sidebands originates from the interaction of the 200- and 700-Hz components.

IV. Bearing Vibration Analysis

While Section III illustrates the effectiveness of the proposed AM detector with simple computer examples, this section uses the AM detector to identify bearing faults in actual machine vibration data. Two new type-6207 bearings are seeded with outer race faults. A point on the outer raceway of one bearing is slightly scratched while a point of the outer raceway of the second bearing is heavily scratched. The third new bearing is left unaltered. From (2) the expected outer raceway fault frequency is calculated as 212 Hz.

The output shaft bearing of a 10-hp NEMA type-215T three-phase 440-V induction motor is replaced by each of the three test bearings in turn. An accelerometer is placed on the stator housing directly above and in the radial direction of the bearing under test. Vibration data are sampled at 10 kHz and divided into 60 records, which are 51.2 ms in length (512 samples each). A Hanning window is then applied to each record. The normalized form of the AM detector from (12) is calculated for each set of bearing data. To perform this calculation, the expressions inside the expectation operators of (12) are applied to each record of data. Next, the results from each record are averaged together as dictated by the expectation operators, and then the remaining expression is evaluated.

When vibration data from the new, undamaged bearing are analyzed, there are no peaks exhibited by the AM detector or the bispectrum. Additionally, there is no energy at any of the characteristic fault frequencies in the power spectrum. Therefore, all three of these tools correctly indicate that there is no fault in the new bearing. Fig. 9 illustrates the results from the bearing whose outer raceway was slightly scratched. The top plot in this figure is the power spectrum estimate. As is common with incipient bearing faults, there is no energy at the characteristic fault frequency, $F_{\mathrm{ORF}} = 212$ Hz, or its multiples. This illustrates the difficulty in detecting incipient bearing faults by directly searching for the characteristic fault frequencies in the power spectrum. The bottom plot in this figure shows the results from the AM detector.

By careful examination of Fig. 9(b) it is seen that there are many peaks occurring at various frequency pairs. However, the vertical axis shows the first row of significant peaks occurs at approximately 212 Hz (the outer raceway fault frequency) and the subsequent row occurs at its next multiple (424 Hz). Also, the

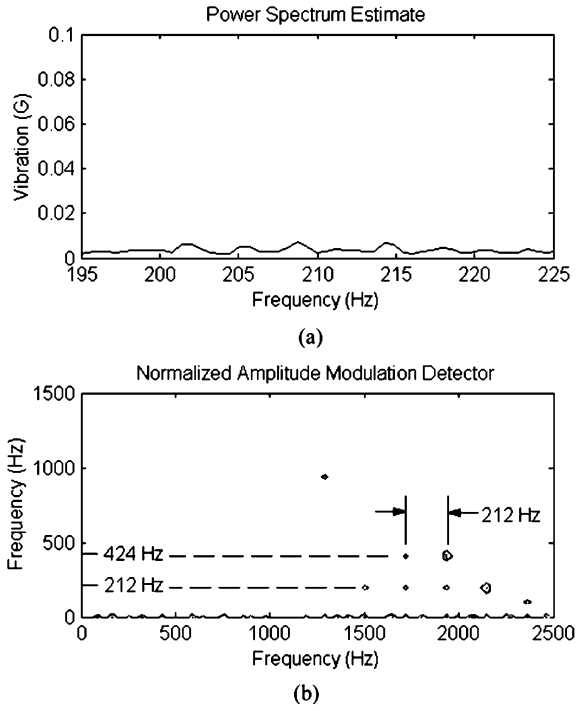

Fig. 9. Detection of an incipient bearing fault. (a) Power spectrum estimate does not exhibit any energy at 212 Hz thereby failing to recognize the fault. (b) The normalized AM detector exhibits several peaks all spaced by $F_{\mathrm{ORF}} = 212$ Hz. This indicates the presence of AM and correctly identifies the presence of an outer raceway defect.

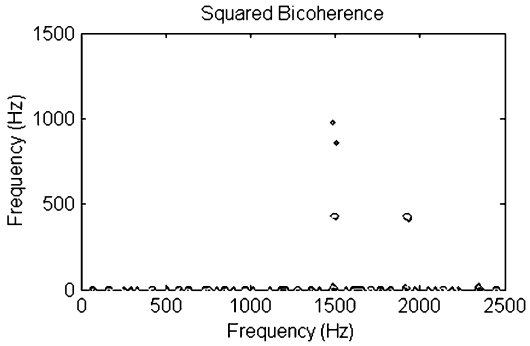

Fig. 10. Squared bicoherence applied to the same bearing vibration data. While a minor amount of QPC is indicated, the arbitrary spacing makes it impossible to determine if this is the result of a bearing fault or some other nonfault source.

spacing of the peaks along the horizontal axis is approximately 212 Hz. The presence of these significant peaks at the characteristic fault frequency in the normalized AM detector correctly indicates the presence of the incipient outer race fault.

To understand how the bispectrum performs when applied to the same vibration data, consider Fig. 10. From this figure, it is evident that the bispectrum is beginning to indicate a minimal amount of QPC; however, the spacing of the peaks is arbitrary. Therefore, it is impossible to determine if these peaks are due to a bearing fault or a result of some other nonfault source. This example illustrates the significantly improved performance of the AM detector over the power spectrum as well as the bispectrum for detecting incipient bearing faults.

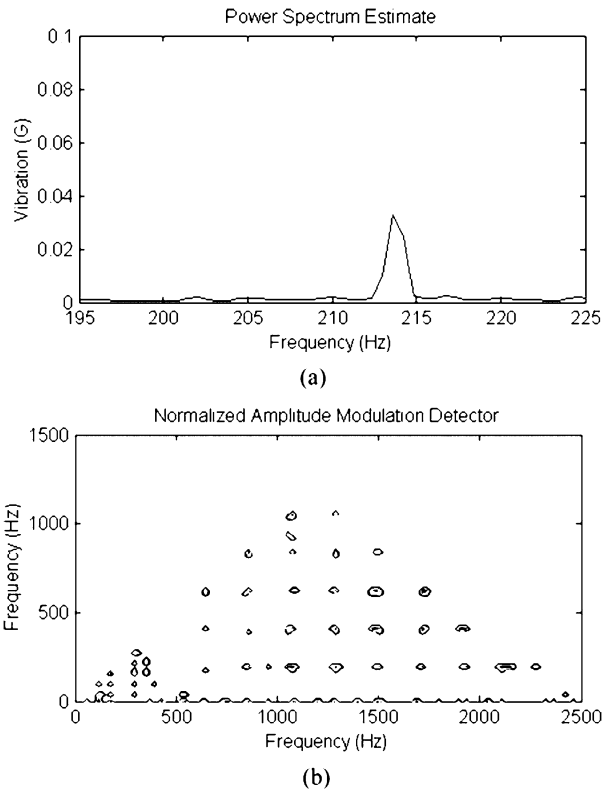

Fig. 11. Detection of an advanced stage bearing fault. (a) Power spectrum estimate exhibits a significant peak near $F_{\mathrm{ORF}} = 212$ Hz. (b) AM detector exhibits a considerable amount of AM. All significant peaks are separated by approximately 212 Hz on the horizontal and vertical axes clearly indicating the presence of a significant outer raceway defect.

Next, consider the application of the AM detector to the bearing with the heavily scratched outer raceway. The severity of this defect is intended to represent a more advanced stage fault. These results are illustrated in Fig. 11. Due to the advanced nature of this defect, a peak near the outer raceway fault frequency is clearly evident in the power spectrum estimate of Fig. 11(a). Because (1)–(4) are functions of θ, it is common for slight amounts of mechanical misalignment (or similar sources) to cause the characteristic fault frequencies to deviate slightly from their exact predicted values. The application of the AM detector to this data is illustrated in Fig. 11(b). In this plot, there is a substantial amount of AM indicated. All significant peaks (above 500 Hz on the horizontal axis) are separated by approximately 212 Hz in the horizontal and vertical directions. This suggests the presence of a significant fault on the outer raceway.

V. Conclusion

This paper has presented a tool for detecting the presence of single-point defect bearing faults. This tool is designed to detect incipient defects before their characteristic fault frequencies become significant in a power spectrum estimate. This is accomplished by searching for instances where the machine's frequencies of mechanical resonance are modulated by the characteristic fault frequencies of the bearing. The AM detector is computed from the machine vibration and its interpretation

only requires knowledge of the bearings characteristic fault frequencies. This method does not require training from various faulted bearings nor does it require baseline data from the machine being monitored. Its proficiency was verified by simulation and experimental results from bearings containing outer race defects.

REFERENCES

[1] "Report of large motor reliability survey of industrial and commercial installations, Part I," *IEEE Trans. Ind. Applicat.*, vol. 21, pp. 853–864, July/Aug. 1985.

[2] "Report of large motor reliability survey of industrial and commercial installations, Part II," *IEEE Trans. Ind. Applicat.*, vol. 21, pp. 865–872, July/Aug. 1985.

[3] P. F. Albrecht, J. C. Appiarius, R. M. McCoy, E. L. Owen, and D. K. Sharma, "Assessment of the reliability of motors in utility applications—Updated," *IEEE Trans. Energy Conversion*, vol. 1, pp. 39–46, Mar. 1986.

[4] O. V. Thorsen and M. Dalva, "Failure and analysis for high-voltage induction motors in the petrochemical industry," *IEEE Trans. Ind. Applicat.*, vol. 35, pp. 810–818, July/Aug. 1999.

[5] R. A. Collacott, *Vibration Monitoring and Diagnosis*. New York: Wiley, 1979, pp. 109–111.

[6] L. Bo, M.-Y. Chow, Y. Tipsuwan, and J. C. Hung, "Neural-network based motor rolling bearing fault diagnosis," *IEEE Trans. Ind. Electron.*, vol. 47, pp. 1060–1068, Oct. 2000.

[7] R. L. Schiltz, "Forcing frequency identification of rolling element bearings," *Sound Vib.*, pp. 16–19, May 1990.

[8] C. L. Nikias and M. R. Raghuveer, "Bispectrum estimation: A digital signal processing framework," *Proc. IEEE*, vol. 75, pp. 869–891, July 1987.

[9] J. W. A. Fackrell, S. McLaughlin, and P. R. White, "Bicoherence estimation using the direct method. Part 1: Theoretical considerations," *Appl. Signal Process.*, vol. 3, pp. 155–168, 1995.

[10] Y. C. Kim and E. J. Powers, "Digital bispectral analysis and its applications to nonlinear wave interactions," *IEEE Trans. Plasma Sci.*, vol. 7, pp. 120–131, June 1979.

[11] P. L. Brockett, M. Hinch, and G. R. Wilson, "Nonlinear and non-Gaussian ocean noise," *J. Acoust. Soc. Amer.*, vol. 82, no. 4, pp. 1386–1394, Oct. 1987.

[12] C. J. Li, J. Ma, and B. Hwang, "Bearing condition monitoring by pattern recognition based on bicoherence analysis of vibrations," *J. Mech. Eng. Sci.*, pt. C, vol. 210, pp. 277–285, 1996.

[13] N. Arthur and J. Penman, "Induction machine condition monitoring with higher order spectra," *IEEE Trans. Ind. Electron*, vol. 47, pp. 1031–1041, Oct. 2000.

[14] A. C. McCormick and A. K. Nandi, "Bispectral and trispectral features for machine condition monitoring," *Proc. IEE—Vis., Image, Signal Process.*, vol. 146, no. 5, pp. 229–234, Oct. 1999.

[15] T. W. S. Chow and H.-Z. Tan, "HOS-Based nonparametric and parametric methodologies for machine fault detection," *IEEE Trans. Ind. Electron.*, vol. 47, pp. 1051–1059, Oct. 2000.

[16] M. R. Raghuveer, "Time-domain approaches to quadratic phase coupling estimation," *IEEE Trans. Automat. Contr.*, vol. 35, pp. 48–56, Jan. 1990.

[17] T. Ning and S. M. Gao, "Detection of amplitude modulation using bispectra," in *Proc. IEEE Int. Conf. Acoustics, Speech, and Signal Processing*, vol. 5, 1992, pp. V469–V472.

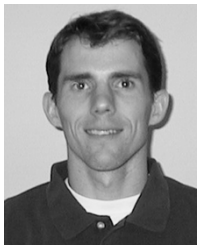

Jason R. Stack (S'94–M'03) received the B.S.E. degree from Mercer University, Macon, GA, in 1996, and the M.S.E. and Ph.D. degrees from Georgia Institute of Technology, Atlanta, in 2000 and 2002, respectively, all in electrical and computer engineering.

He is currently a Research Engineer in the Signal and Image Processing Branch, Naval Surface Warfare Center, Panama City, FL. His research interests include condition monitoring, autonomous systems, applied artificial intelligence, and pattern recognition. Before beginning his graduate studies, he was a Design Engineer with Exide Electronics, Raleigh, NC, where he designed uninterruptible power supplies. He has also been a Design Eengineer developing electric, hydraulic, and pneumatic control systems.

Ronald G. Harley (M'77–SM'86–F'92) was born in South Africa. He received the B.Sc.Eng. (*cum laude*) and M.Sc.Eng. (*cum laude*) degrees from the University of Pretoria, Pretoria, South Africa, in 1960 and 1965, respectively, and the Ph.D. degree from London University, London, U.K., in 1969.

In 1971, he was appointed to the Chair of Electrical Machines and Power Systems at the University of Natal, Durban, South Africa. He was a Visiting Professor at Iowa State University, Ames, in 1977, at Clemson University, Clemson, SC, in 1987, and at Georgia Institute of Technology, Atlanta, in 1994. He is currently the Duke Power Company Distinguished Professor at Georgia Institute of Technology. His research interests include the dynamic behavior and condition monitoring of electric machines, motor drives, and power systems, and controlling them by the use of power electronics and intelligent control algorithms. He has coauthored some 280 papers published in refereed journals and international conference proceedings, of which nine have received prizes.

Dr. Harley was elected as a Distinguished Lecturer by the IEEE Industry Applications Society (IAS) for the years 2000 and 2001. He is currently the Vice-President of Operations of the IEEE Power Electronics Society, and the Chair of the Distinguished Lecturers and Regional Speakers Program of the IAS. He is a Fellow of the Institution of Electrical Engineers, U.K., and the Royal Society in South Africa, and a Founder Member of the Academy of Science in South Africa formed in 1994.

Thomas G. Habetler (M'83–SM'92–F'02) received the B.S.E.E. and M.S. degrees in electrical engineering from Marquette University, Milwaukee, WI, in 1981 and 1984, respectively, and the Ph.D. degree from the University of Wisconsin, Madison, in 1989.

From 1983 to 1985, he was with the Electro-Motive Division, General Motors, as a Project Engineer. While there, he was involved in the design of switching power supplies and voltage regulators for locomotive applications. He is currently a Professor of Electrical Engineering at Georgia Institute of Technology, Atlanta. His research interests are in switching converter technology and electric machine protection and drives.

Dr. Habetler received the 1989 First-Prize Paper Award and 1991 Second-Prize Paper Award of the Industrial Drives Committee of the IEEE Industry Applications Society (IAS), and the 1994 and 2001 Second-Prize Paper Awards of the IAS Electric Machines Committee. He served as the President of the IEEE Power Electronics Society from 2001 to 2002. He serves as the Chair of the IAS Industrial Power Converter Committee.